Supplementary information for

Revisiting Charge Transport in Spiro-OMeTAD using Space-Charge-Limited Current Measurements

by J. A. Röhr *et al*.

This supplementary information (SI) contains the derivation of key equations in the main text, namely eq. 4 (the current at low voltages when a built-in voltage is present) and eq. 6 (the moving electrode equations). The SI also contains a description of the performed drift-diffusion simulations along with some preliminary drift-diffusion results showing the effect of a built-in voltage and/or exponential tails on single-carrier device *J*-*V* curves. Furthermore, additional fitting results are shown, namely for the temperature series of a 115, 190 and 290 nm single carrier device, and fits to asymmetric *J*-*V* curves using analytical equations. Finally, the SI contains a detailed analysis of the accuracy of eq. 17 in the main text compared to the Mark-Helfrich equation[1]. References are included where needed.

The content of the SI is not necessary to understand the key message of the paper, but is merely included for the interested reader.

1 Derivation of eq. 4 and eq. 6 in the main text

The one dimensional drift-diffusion equation for positively charged carriers (holes) is given by,

$$\frac{J_p}{q} = -D_p \frac{dp}{dx} + p\mu_p F \qquad \text{(S1)}$$

where J_p is the current density, q is the elementary charge, D_p is the diffusion coefficient, p is the hole density, μ_p is the hole mobility and F is the electric field. By rewriting the equation on the form of a first-order differential equation (in terms of the charge carrier mobility and the valence band edge) we obtain,

$$\frac{dp(x)}{dx} - p(x)\frac{1}{k_\mathrm{B}T}\frac{dE_\mathrm{V}(x)}{dx} = -\frac{J_p}{\mu_p k_\mathrm{B}T}. \qquad \text{(S2)}$$

We can multiply both sides of eq. S2 with the integration factor, $e^{-\frac{1}{k_\mathrm{B}T}\int\frac{dE_\mathrm{V}(x)}{dx}dx}$,

$$\left(\frac{dp(x)}{dx} - p(x)\frac{1}{k_\mathrm{B}T}\frac{dE_\mathrm{V}(x)}{dx}\right)e^{-\frac{1}{k_\mathrm{B}T}\int\frac{dE_\mathrm{V}(x)}{dx}dx} = \left(-\frac{J_p}{\mu_p k_\mathrm{B}T}\right)e^{-\frac{1}{k_\mathrm{B}T}\int\frac{dE_\mathrm{V}(x)}{dx}dx}. \qquad \text{(S3)}$$

The left hand side of eq. S3 can be rewritten through the reverse product rule,

$$\frac{d}{dx}p(x)e^{-\frac{1}{k_\mathrm{B}T}\int\frac{dE_\mathrm{V}(x)}{dx}dx} = \left(-\frac{J_p}{\mu_p k_\mathrm{B}T}\right)e^{-\frac{1}{k_\mathrm{B}T}\int\frac{dE_\mathrm{V}(x)}{dx}dx} \quad \text{(S4)}$$

and by integration of both sides over the whole space-charge region (0 to L), and by using the corollary theorem of calculus, we obtain,

$$-\mu_p k_\mathrm{B}Tp(x)e^{-\frac{1}{k_\mathrm{B}T}\int_0^L\frac{dE_\mathrm{V}(x)}{dx}dx}\Big|_0^L = J_p\int_0^L e^{-\frac{1}{k_\mathrm{B}T}\int_0^L\frac{dE_\mathrm{V}(x)}{dx}dx}\,dx. \quad \text{(S5)}$$

For large built-in voltages, the valence band edge will depend linearly on the spatial position inside the semiconductor, and is given by,

$$E_\mathrm{V} = -q\left\{V + \phi_\mathrm{inj}\left(1-\frac{x}{L}\right) + (\phi_\mathrm{ext} - V)\frac{x}{L}\right\} \quad \text{(S6)}$$

which yield the boundary conditions for the valence band edge,

$$E_\mathrm{V}(0) = -q(V + \phi_\mathrm{inj}), \quad \text{(S7)}$$

$$E_\mathrm{V}(L) = -q\phi_\mathrm{ext}. \quad \text{(S8)}$$

The boundary conditions for the charge carrier density is given by the injection barrier heights and the effective density of states (assuming Boltzmann statistics),

$$p(0) = N_V \exp\left(-\frac{q\phi_\mathrm{inj}}{k_\mathrm{B}T}\right) \quad \text{(S9)}$$

$$p(L) = N_V \exp\left(-\frac{q\phi_\mathrm{ext}}{k_\mathrm{B}T}\right) \quad \text{(S10)}$$

The left hand side of eq. S5 can now be evaluated by using the boundary conditions for the conduction band edge (eq. S7 & S8) and the boundary conditions for the charge-carrier density (eq. S9 & S10), whereas the right hand side of the eq. S5 must be evaluated using eq. S6 (note that the integrals inside the exponentials can be evaluated using the corollary. i.e., simply from considering the boundary conditions). This evaluation leads to,

$$J_p = \frac{q\mu_{\mathrm{h}} N_{\mathrm{V}} (\phi_{\mathrm{ext}} - \phi_{\mathrm{inj}} - V)\left\{\exp\left(\frac{qV}{k_{\mathrm{B}}T}\right) - 1\right\}}{L \exp\left(\frac{q\phi_{\mathrm{inj}}}{k_{\mathrm{B}}T}\right)\left\{\exp\left(\frac{q\phi_{\mathrm{ext}} - q\phi_{\mathrm{inj}}}{k_{\mathrm{B}}T}\right) - \exp\left(\frac{qV}{k_{\mathrm{B}}T}\right)\right\}} \qquad \text{(S12)}$$

which is the general expression for the trap-free drift-diffusion hole current density in a single-carrier device neglecting band bending at the interface (flat band picture) where $\phi_{\mathrm{ext}} - \phi_{\mathrm{inj}} = V_{\mathrm{bi}}$. With $\phi_{\mathrm{inj}} = \phi_{\mathrm{ext}} = 0$ the general expression reduces to,

$$J = q\mu_{\mathrm{h}} N_{\mathrm{V}} \frac{V}{L} \qquad \text{(S13)}$$

which is Ohm's law in the saturation limit[2]. When the injection barrier heights are non-zero and of similar height $\phi_{\mathrm{inj}} = \phi_{\mathrm{ext}} > 0$, the general expression reduces to,

$$J = q\mu_{\mathrm{h}} N_{\mathrm{V}} \frac{V}{L} \exp\left(-\frac{q\phi_{\mathrm{inj/ext}}}{k_{\mathrm{B}}T}\right) \qquad \text{(S14)}$$

which is Ohm's law in the saturation regime corrected by the injection barriers. Eq. S14 is only truly valid when $\phi_{\mathrm{inj/ext}} > 2k_{\mathrm{B}}T$, and close to degeneracy S13 must be corrected by a term allowing for Fermi-Dirac statistics. When the built-in voltage is low, the built-in voltage is reduced due to band bending at the injecting interface. We denote this reduction in voltage as b. We can modify eq. S12 to take this reduction into account by changing the boundary conditions to,

$$E_{\mathrm{V}} = -q\left\{V + (\phi_{\mathrm{inj}} + b)\left(1 - \frac{x}{L}\right) + (\phi_{\mathrm{ext}} - V)\frac{x}{L}\right\} \qquad \text{(S15)}$$

$$E_{\mathrm{V}}(0) = -q(V + \phi_{\mathrm{inj}} + b), \qquad \text{(S16)}$$

$$E_{\mathrm{V}}(L) = -q\phi_{\mathrm{ext}}. \qquad \text{(S17)}$$

$$p(0) = N_V \exp\left(-\frac{q(\phi_{\mathrm{inj}} + b)}{k_{\mathrm{B}}T}\right) \qquad \text{(S18)}$$

$$p(L) = N_V \exp\left(-\frac{q\phi_{\mathrm{ext}}}{k_{\mathrm{B}}T}\right) \qquad \text{(S19)}$$

which yields,

$$J_{\mathrm{p}} = \frac{q\mu_{\mathrm{h}} N_{\mathrm{V}} (\phi_{\mathrm{ext}} - \phi_{\mathrm{inj}} - b - V)\left\{\exp\left(\frac{qV}{k_{\mathrm{B}}T}\right) - 1\right\}}{L \exp\left(\frac{q\phi_{\mathrm{inj}}}{k_{\mathrm{B}}T}\right)\exp\left(\frac{qb}{k_{\mathrm{B}}T}\right)\left\{\exp\left(\frac{q\phi_{\mathrm{ext}} - q\phi_{\mathrm{inj}} - qb}{k_{\mathrm{B}}T}\right) - \exp\left(\frac{qV}{k_{\mathrm{B}}T}\right)\right\}} \qquad \text{(S20)}$$

which is eq. 4 in the main text. At low built-in voltages, a proposed approximation of b is given by[3,4],

$$b = \frac{k_B T}{q}\left\{\ln\left(\frac{q^2 N_V L^2}{2 k_B T \varepsilon_r \varepsilon_0}\right) - 2\right\}. \qquad \text{(S21)}$$

However, for the built-in voltages estimated in this study (≥ 0.8 V), b can usually be neglected. From eq. S20 we can derive the moving electrode (ME) equation[5,6,7]. The ME equation assumes that $q\phi_{ext} = q\phi_{inj} = 0$, reducing S20 to,

$$J = \frac{q\mu_h N_V(-b-V)\left\{\exp\left(\frac{qV}{k_B T}\right)-1\right\}}{L\exp\left(\frac{qb}{k_B T}\right)\left\{\exp\left(\frac{-qb}{k_B T}\right)-\exp\left(\frac{qV}{k_B T}\right)\right\}} \qquad \text{(S22)}$$

We can neglect b by realising that the magnitude of the carrier density is dominated by the density in the middle of the device. The carrier density in a symmetric single-carrier device can be approximated by[7],

$$p(x) = \frac{2\pi^2 \varepsilon_r \varepsilon_0 k_B T}{q^2 L^2} \frac{1}{\cos^2\left[\pi\left(\frac{x}{L}-\frac{1}{2}\right)\right]} \qquad \text{(S23)}$$

which yields a carrier density in the middle of the device, $p_0 = n(L/2)$, which is given by,

$$p_0 = \frac{2\pi^2 \varepsilon_r \varepsilon_0 k_B T}{q^2 L^2}. \qquad \text{(S24)}$$

Finally, we replace N_V with $2p_0$ and set b = 0 in eq. S22, and we obtain the ME equation[5,6,7],

$$J = 4\pi^2 \frac{k_B T}{q} \varepsilon_r \varepsilon_0 \mu_h \frac{V}{L^3}. \qquad \text{(S25)}$$

2 Drift-diffusion simulations

The simulations of the current density-voltage profiles of the single-carrier devices were performed using commercially available device simulator called Advanced Semiconductor Analysis (ASA), which solves Poisson's equation and the drift-diffusion equations for electrons and holes[8],

$$\nabla^2\varphi = -\frac{\rho}{\varepsilon_r\varepsilon_0} \qquad \text{(S26)}$$

$$-\frac{1}{q}J_n = -D_n\frac{dn}{dx} - n\mu_n F \qquad \text{(S27)}$$

$$\frac{1}{q}J_p = -D_p\frac{dp}{dx} + p\mu_p F \qquad \text{(S28)}$$

where φ is the electric potential, ρ is the space-charge density, $\varepsilon_r\varepsilon_0$ is the permittivity, q is the elementary charge, J_n and J_p are the current densities for electrons and holes respectively, D_n and D_p are the diffusion coefficients, n and p are the charge-carrier densities, μ_n and μ_p are the charge-carrier mobilities, and F is the electric field. The boundary conditions for the simulations are set by the device boundaries through the injection and extraction barrier heights, $q\phi_{inj}$ and $q\phi_{ext}$, which in turn defines the built-in voltage, V_{bi} (figure 1c), through,

$$qV_{bi} = q\phi_{ext} - q\phi_{inj}. \quad \text{(S29)}$$

Shallow trap states due to energetic disorder can be modelled through the inclusion of an exponential density of states from the transport level into the band gap. The density of the conduction band tails, h_{CBT}, and valence band tails, h_{VBT}, are given by,

$$h_{CBT} = n_{t,n}\exp\left(-\frac{E_C - E}{E_{ch,n}}\right) \qquad \text{(S30)}$$

$$h_{VBT} = n_{t,p}\exp\left(-\frac{E - E_V}{E_{ch,p}}\right) \qquad \text{(S31)}$$

where $n_{t,n}$ and $n_{t,p}$ are the trap densities per unit energy, E_C and E_V are the conduction and valence band edge values, respectively, and $E_{ch,n}$ and $E_{ch,p}$ are the characteristic energies which defines the energetic depths of the exponential tails. We utilize a multiple trapping-release model where all charge carriers in the extended states within the gap are immobile, such that transport can only take place at the band edge. Shockley-Read-Hall statistics was used to model the trap occupancies, which assumes that charge carriers are trapped at a rate which is energy independent and thermally de-trapped at a rate which is field independent. Since this study involves hole-only devices, the tails density and characteristic energy will only be presented for holes. A more detailed description of the simulations can be found in the literature[8,9,10].

The slope of the *J-V* curve of a log-log scale, m, can be derived by,

$$m = \frac{d \log J}{d \log V} \qquad \text{(S32)}$$

where m will be unity for linear currents and m will be 2 when the current follows the Mott-Gurney law. The slope function is therefore a convenient tool for analysing different voltage regimes. It is well-known that the slope will take a higher value than 2 when traps are present[11].

A shunt current is defined as an unwanted current flowing between the front and back electrode. This is usually caused by diffusion of metal through the probe material during fabrication or at very high applied electric fields, giving rise to Ohmic current pathways. We can model this by allowing for a parallel current to flow alongside our SCLC current, which is defined by the shunt (or parallel) resistance, R_P. Since the shunt resistance is the resistance hindering the shunt current, a large shunt resistance is usually desired for electronic devices.

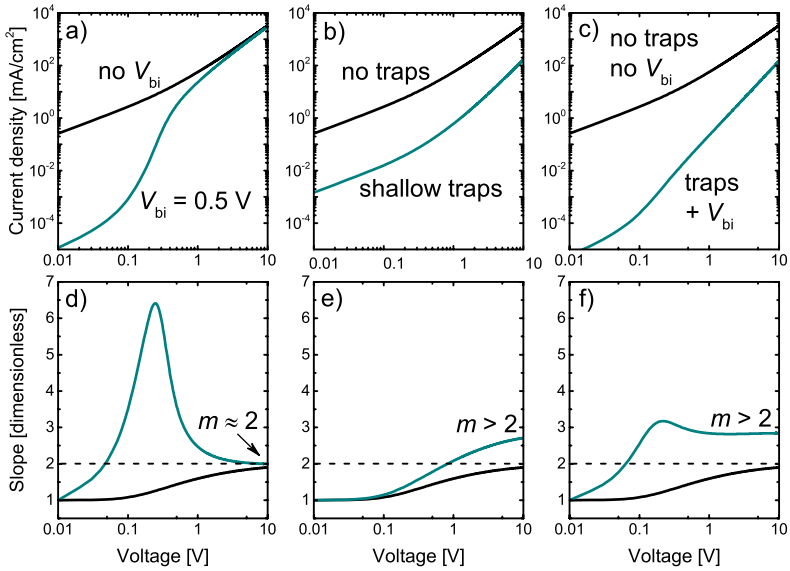

Figure S1 – Drift-diffusion simulations of *J-V* curves of single-carrier devices with a) built-in potential of 0.5 V, b) traps in the form of exponential tails (E_{ch} = 0.050 eV and $N_{tails} = 5 \cdot 10^{19}$ cm^{-3} eV^{-1}), and c) a combination of a built-in potential and traps. d-f) show the corresponding slope plots of a-c). The dashed line represents the slope value of the Mott-Gurney law.

In order to elucidate the effect of a built-in voltage and shallow traps in combination, drift-diffusion simulations of 2 eV band gap 100 nm single-carrier devices were performed. Figure S1 shows the result of drift-diffusion simulations where the charge-carrier mobility was arbitrarily chosen to be 10^{-4} cm^2/Vs. However, the charge-carrier mobility only affects the magnitude of the current density and not the voltage regimes. Figure S1a shows the simulated *J-V* curves of a single-carrier device with and without a built-in voltage of 0.5 V. The built-in voltage introduces an energetic barrier for the charge-carriers to overcome in forward bias before drift currents can dominate the *J-V* curve, whereas the reverse bias current will be injection limited (with a barrier height of qV_{bi}). The energetic barrier manifests itself by an exponential increase of the current density on a log-log scale. The corresponding *m-V* curves for fig. S1a are seen in fig. S1d, where

the slope is seen to have a large peak until reaching the slope ($m \approx 2$) of the device without a built-in voltage. This peak in the *m-V* curve can be used as an additional fitting landmark to help extract the built-in voltage. Figure S1b shows the *J-V* curves with and without traps in the form of exponential tails ($E_{\mathrm{ch}} = 0.050$ eV and $n_{\mathrm{t}} = 5 \cdot 10^{19}$ cm^{-3}eV^{-1}). The traps are seen to lower the current across the entire voltage range due to the lowering of the number of free charge-carriers present for conduction. Figure S1e shows the corresponding *m-V* curves to fig. S1b, where the slope at high voltages is seen to approach a value substantially higher than $m \approx 2$ which is a clear indication that we cannot analyse these curves using the Mott-Gurney law. Figure S1c shows the *J-V* curve for when a combination of traps and a built-in voltage is present. We see that the built-in voltage, in this case, dominates at low voltages whereas the traps dominate at higher voltages. That the built-in voltage dominates at low voltages is of course completely dependent on the choice of the values chosen for the simulation. However, given that the built-in voltage is high and the trap density and characteristic energy is low, one can assume that the built-in voltage will be the dominant factor. The corresponding *m-V* curves to fig. S1c is shown in fig. S1f, where the peak due to the built-in voltage is slightly lowered due to the presence of traps. Most importantly, the slope at high voltages still takes a value which is larger than what is expected from the Mott-Gurney law. So from considering the *m-V* curves alone we can already determine that the transport in the device is governed by traps in the form of exponential tails and that there is a substantial built-in voltage.

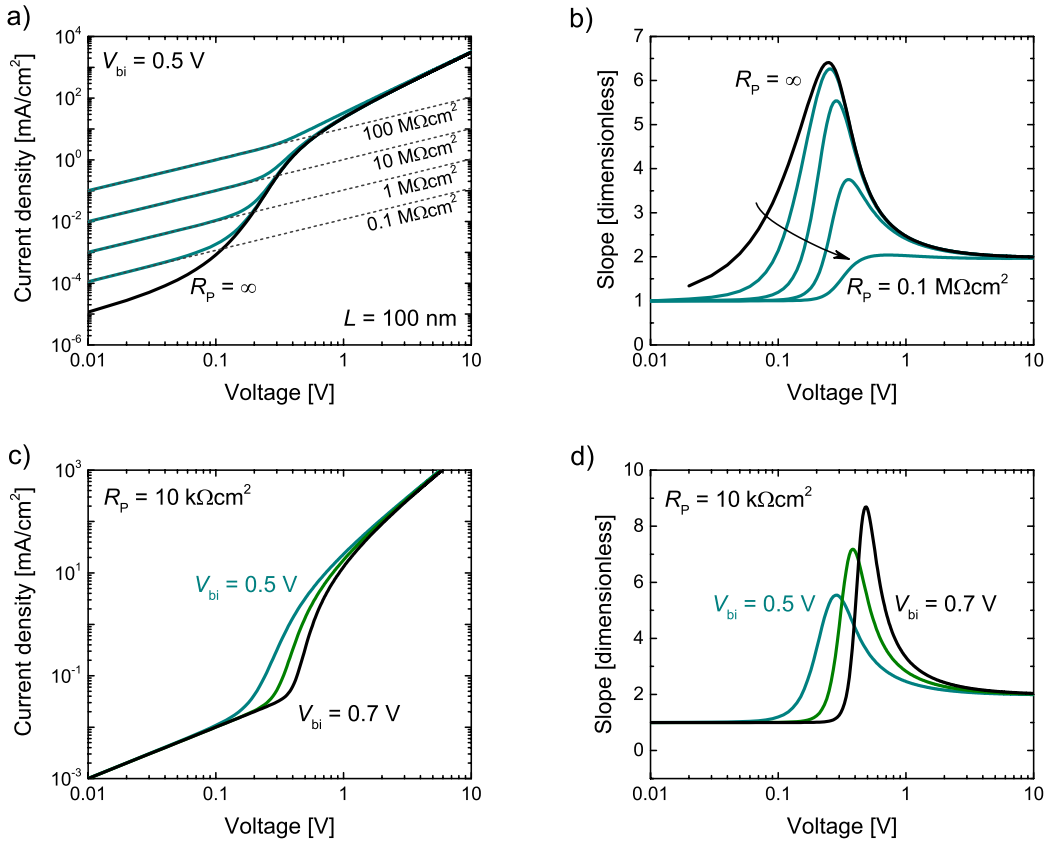

Figure S2 – Drift-diffusion simulations of a) *J-V* curves of an asymmetric single-carrier device with decreasing shunt resistance, i.e., increasing shunt current, and b) corresponding *m-V* curves. c) Simulated *J-V* curves with a fixed shunt resistance, and d) corresponding *m-V* curves.

Figure S2 shows the effect on simulated *J-V* curves and the corresponding *m-V* curves, of a trap-free asymmetric single-carrier device with a built-in voltage of 0.5 V present, when the shunt

resistance is lowered (the situation $R_P = \infty$ is when no shunt current is present). By comparing fig. S1a with fig. S2a we see that where the increase of the current of the asymmetric device without a shunt current is seen to increase exponentially on a log-log scale, the addition of a shunt current is acting to linearize the current density at low voltages. Consequently, if the shunt resistance is so low that it completely masks the space-charge limited current, the device is considered completely short-circuited, and the current across the device will be due to shunt pathways only. The linearization of the current can also be seen from fig. S2b where the slope is seen to remain linear up to higher voltages. Additionally, the sharpness of the peak caused by the built-in voltage is seen to increase while the magnitude of the peak is seen to decrease as the shunt resistance is decreased (the peak ultimately disappears when the current is completely linear with voltage). A very sharp peak can then be attributed to a combination of a large built-in voltage and the presence of a shunt current, and we can, as before, use this peak as an additional fitting landmark. Figure 3c is showing the effect of increasing the built-in voltage given that the shunt resistance is low enough to mask the effect of the V_{bi} at low voltages. The onset to a higher order current-voltage dependence is seen to shift to higher voltages along with an overall increase of the slope (fig. S2d).

3 Additional fitting results

The following section contains additional fits and fitting results of SCLC temperature series at three different thicknesses (115 nm, 190 nm and 290 nm). Each *J-V* plot is accompanied by a plot showing the band edge mobility, a plot showing the characteristic energy, and a plot showing the trap density, all of them as a function of temperature and injection barrier height. It should here be noted, that a consistent fit across all thicknesses and temperatures could not be achieved without the inclusion of both exponential tails and injection barrier heights as presented. The band edge mobility show a small increase with increase in temperature (for all three thicknesses), whereas the trap density was seen to decrease with less than a factor of 2 from 200K to 300K (for all thicknesses). The characteristic energy was found to be primarily unaffected by the change in temperature.

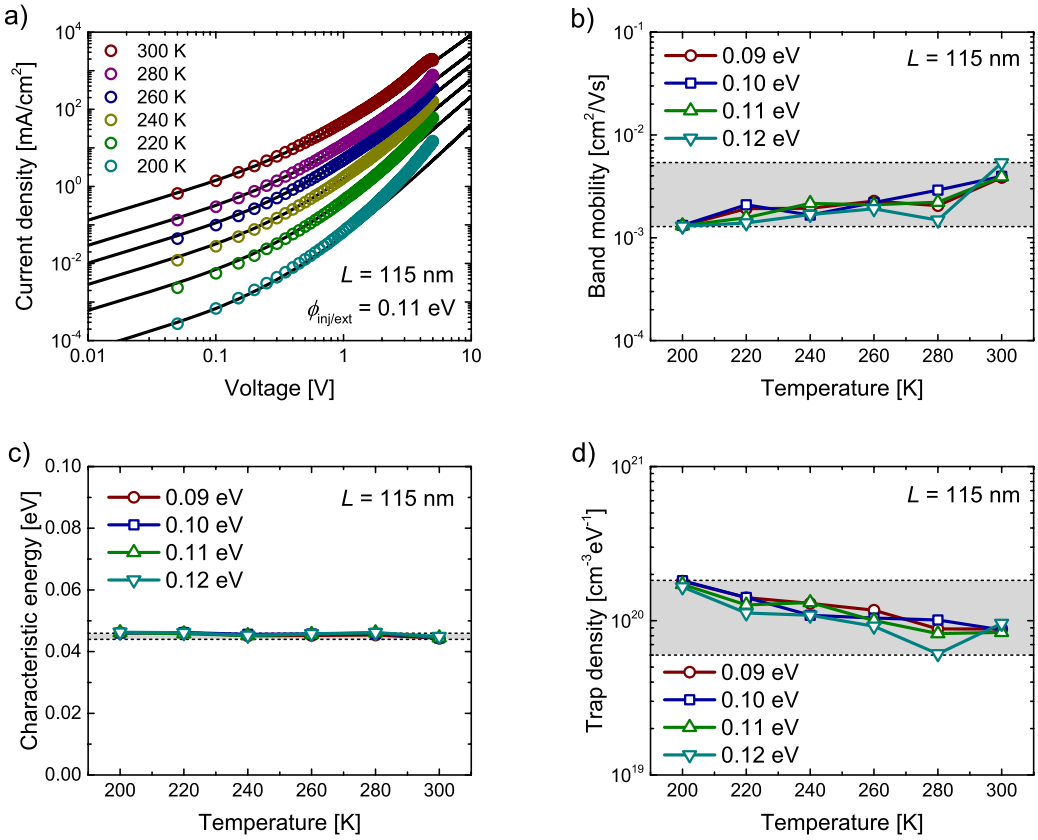

Figure S3 – Fitting results to the SCLC temperature series of a 115 nm device. a) Experimental and fitted *J-V* curves (using an injection barrier height of 0.11 eV and the corresponding mobility and trap characteristics), b) obtained band mobility, c) characteristic energy of exponential tail states, and d) exponential trap density at varying injection barrier heights (0.09 eV to 0.12 eV) and temperature (200K to 300K).

Figure S3 shows the fitting results to the temperature series of a 115 nm device. The inclusion of injection barriers were needed in order to fit to the whole temperature series without significant variation of both the band mobility, characteristic energy and the trap density. Minimal variation was obtained when an injection barrier between 0.09 eV and 0.12 eV was included. Figure S3a shows the resulting fits to the experimentally obtained *J-V* curves (both the experimental and fitted curves are shown on a log-log scale). The best fits were obtained using injection barrier heights for both injection and extraction of 0.11 eV. Figure S3b shows the resulting band hole-mobility as a function of temperature at different injection barrier heights. A slight increase of the mobility with temperature is observed. Figure S3c shows the resulting characteristic energy. No significant variation was observed with increasing temperature. Figure S3c shows the resulting trap density. Where the hole-mobility was seen to increase with temperature, the trap density was seen to decrease with temperature.

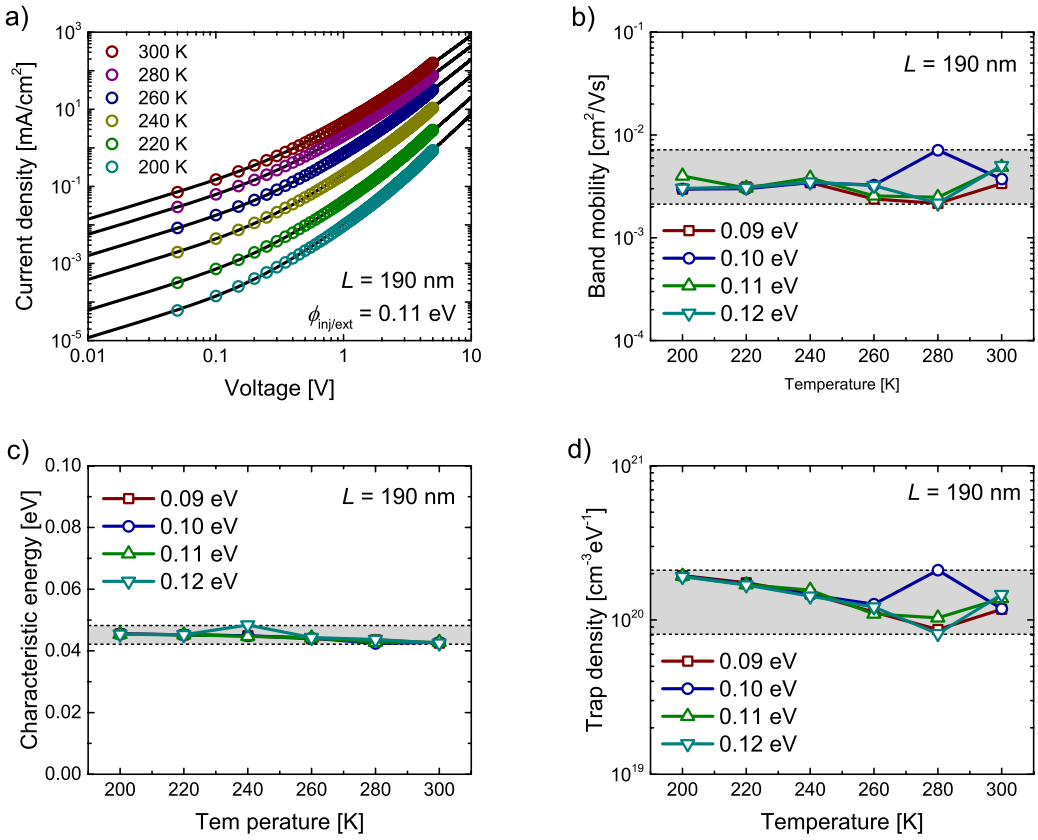

Figure S4 – Fitting results to the SCLC temperature series of a 190 nm device. a) Experimental and fitted *J-V* curves (using an injection barrier height of 0.11 eV and the corresponding mobility and trap characteristics), b) obtained band mobility, c) characteristic energy of exponential tail states, and d) exponential trap density at varying injection barrier heights (0.09 eV to 0.12 eV) and temperature (200K to 300K).

Figure S4 shows the fitting results to the temperature series of a 190 nm device. Similar to the 115 nm case, the inclusion of injection barriers were needed in order to fit to the whole temperature series without significant variation of both the band mobility, characteristic energy and the trap density. Minimal variation was obtained when an injection barrier between 0.09 eV and 0.12 eV was included. Figure S4a shows the experimental data along with the fits. Figure S4b, c, and d shows the resulting band hole-mobility, characteristic energy and trap density obtained from the fits. Contrary to the 115 nm case, the 190 nm case does not show a significant increase of the mobility with temperature. A decrease in the trap density was however observed with increased temperature as with the 115 nm case.

Figure S5 shows similar fits for a 290 nm device as was shown for a 115 nm and a 190 nm device in figure S3 and S4. Similar to the 115 nm device, the mobility is seen to increase with temperature while the trap density is decreasing with temperature.

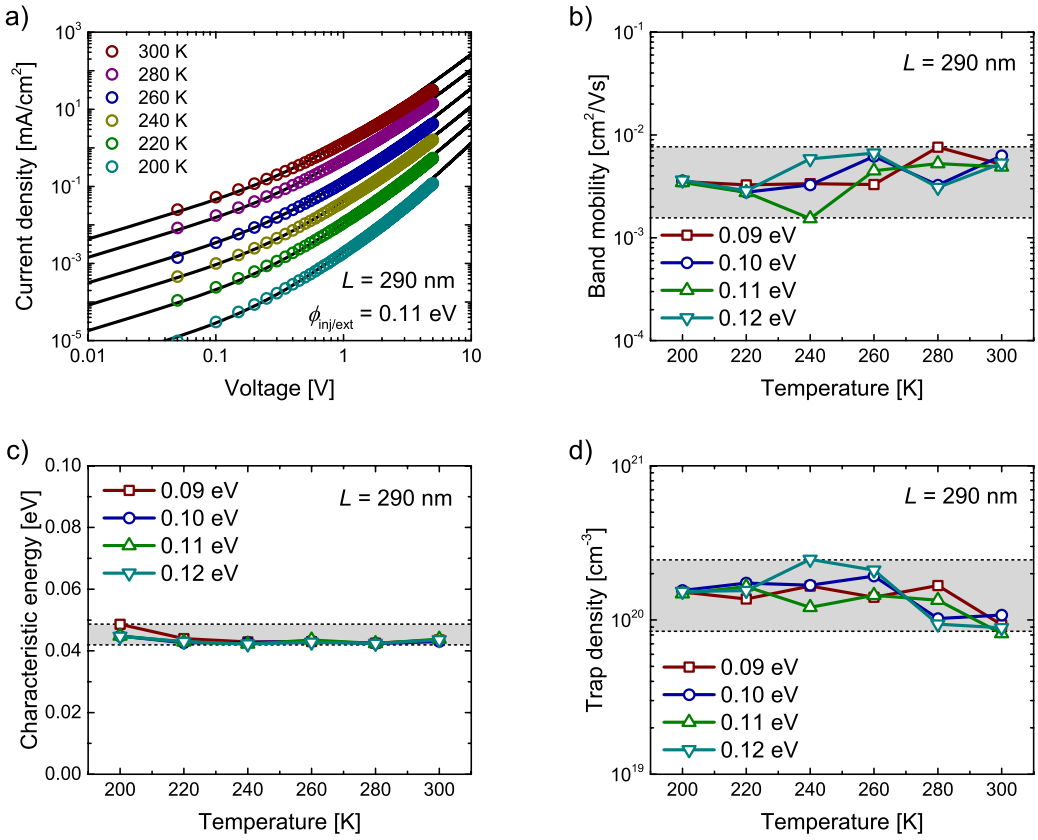

Figure S5 – Fitting results to the SCLC temperature series of a 290 nm device. a) Experimental and fitted *J-V* curves (using an injection barrier height of 0.11 eV and the corresponding mobility and trap characteristics), b) obtained band mobility, c) characteristic energy of exponential tail states, and d) exponential trap density at varying injection barrier heights (0.09 eV to 0.12 eV) and temperature (200K to 300K).

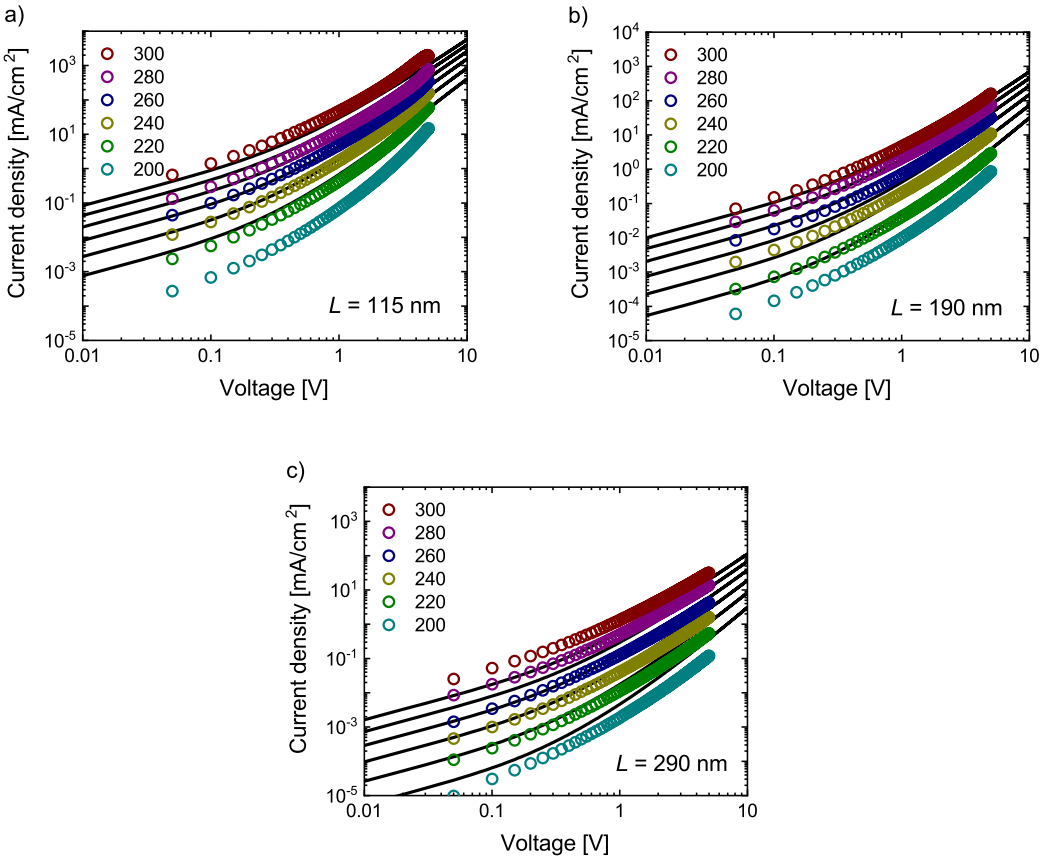

Figure S6 – Comparison between SCLC data and the drift-diffusion simulations when fitting the entire data set with a single set of (temperature independent) parameters. E_g = 3 eV, ε_r = 3, N_V = 10^{19} cm^{-3}, μ_h = 3.5 · 10^{-3} cm^2/Vs, $q\phi_{inj}$ = $q\phi_{ext}$ = 0.11 eV, E_{ch} = 0.045, n_t = 10^{20} cm^{-3}eV^{-1}. a) 115 nm, b) 190 nm, and c) 290 nm.

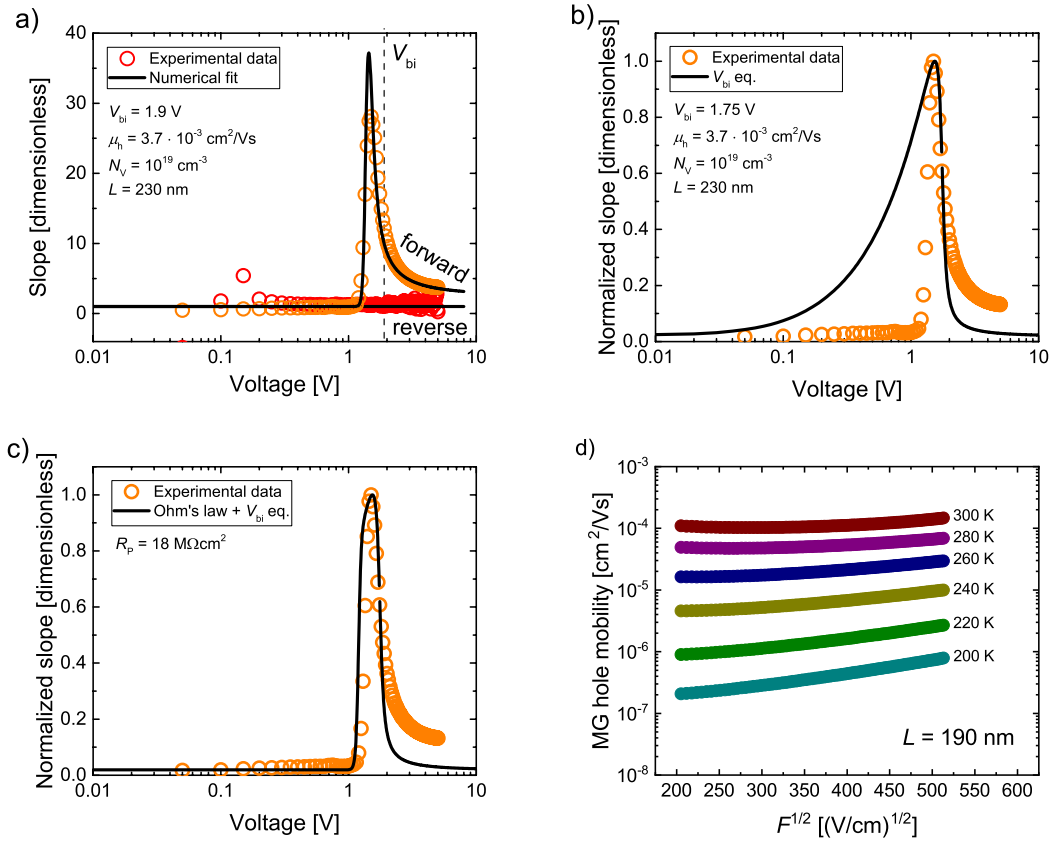

Figure S7 – a) Numerical fits to *m*-*V* data from the asymmetrical Spiro-OMeTAD device *J*-*V* curves, obtaining a built-in voltage of 1.9 V. Normalized fit of eq. 4 to b) Spiro-OMeTAD device data, obtaining a built-in voltage of 1.75 V. The peak of the slope (*m*) of eq. 4 is uniquely defined by the built-in voltage. Normalized fit using a sum of eq. 4 and eq. 7 (Ohm's law) to c) Spiro-OMeTAD data. d) Apparent field dependence observed when fitting with the Mott-Gurney law across the entire voltage range.

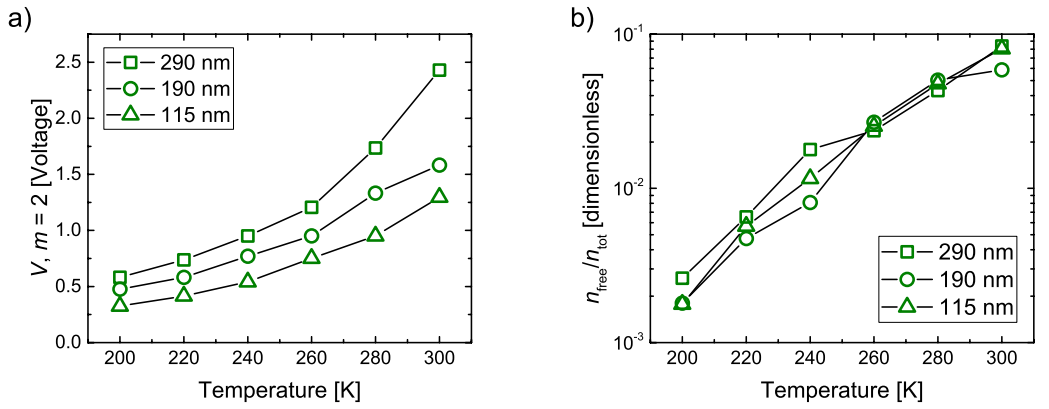

Figure S8 – a) The value of the voltage where m = 2 (point of evaluation of the Mott-Gurney law). b) Ratio of average values of the free to total (free + trapped) charge carrier densities evaluated at the voltages in a).

3 Accuracy of eq. 17

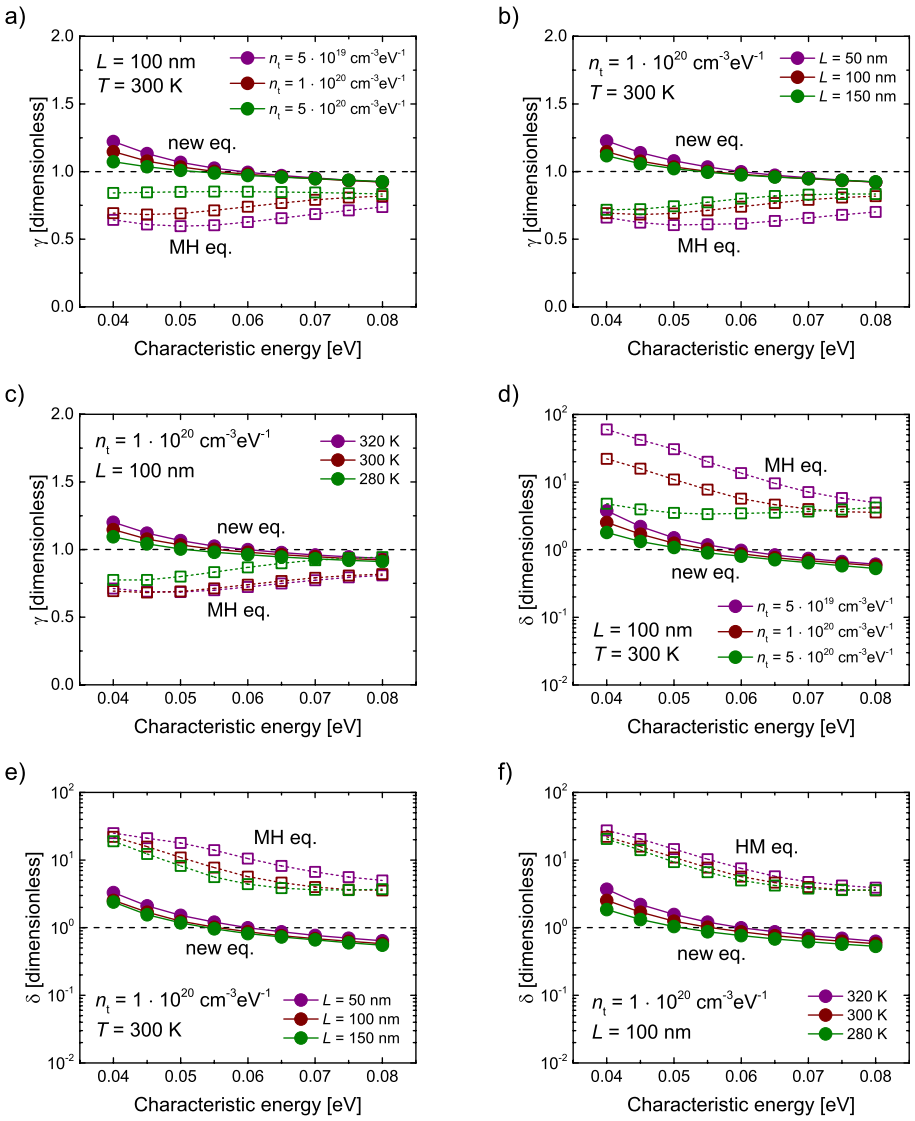

Figure S9 – Accuracy of eq. 17 compared to the MH equation in terms of match between the input values for the trap characteristics to the output values obtained from the equations, γ and δ, when the mobility is kept fixed. The trap density, semiconductor thickness and temperature was varied.

In order to evaluate how well eq. 17 determines the trap characteristics, the equation is fitted to *J-V* curves generated from drift-diffusion simulations of symmetric single-carrier devices containing traps in the form of exponential tails. We compare these fitting results to fits of the same curves using the Mark-Helfrich equation. We examine how the fitting values of E_{ch} and N_{t} compare to the input values of the same parameters,

$$\gamma = \frac{E_{\mathrm{ch}}^{\mathrm{out}}}{E_{\mathrm{ch}}^{\mathrm{in}}} \quad \text{and} \quad \delta = \frac{N_{\mathrm{t}}^{\mathrm{out}}}{N_{\mathrm{t}}^{\mathrm{in}}}. \qquad \text{(S33)}$$

Figure S9 shows γ and δ as a function of the characteristic energy when either the trap density, the semiconductor thickness or the temperature is varied. The following values were kept fixed during the fitting procedures with both the numerical simulations and the equations: $N_{\mathrm{eff}} = 10^{20}$ cm^{-3}eV^{-1}, $E_{\mathrm{g}} = 2$ eV and $\mu = 10^{-4}$ cm^2/Vs.

Figure S9a), b) and c) shows the ratio of characteristic energy obtained from fitting equation 17 and the MH equation compared to the input characteristic energy as this energy is varied. A very small deviation from unity is seen in all examples when eq. 17 is used, indicating that the low voltage *J-V* curve can be very well reproduced. Moreover, the ratios are seen to converge for large values of the characteristic energy. Figure S9c), e) and f) shows the ratio of the trap density obtained from fitting to the input trap density using eq. 17. In all cases the trap density is estimated within an order of magnitude. Where excellent agreement is found with eq. 17, the results using the MH equation are seen to deviate dramatically.

4 References

[1] P. Mark and W. Helfrich, J. Appl. Phys. **33**, 205 (1962).

[2] J.G. Simmons, Phys. Rev. Lett. **15**, 967 (1965).

[3] J.G. Simmons, J. Phys. Chem. Solids **32**, 1987 (1971).

[4] P. De Bruyn, A.H.P. Van Rest, G.A.H. Wetzelaer, D.M. De Leeuw, and P.W.M. Blom, Phys. Rev. Lett. **111**, 1 (2013).

[5] R. de Levie, N.G. Seidah, and H. Moreia, J. Membr. Biol. **10**, 171 (1972).

[6] A.A. Grinberg and S. Luryi, J. Appl. Phys. **61**, 1181 (1987).

[7] S.L.M. van Mensfoort and R. Coehoorn, Phys. Rev. B **78**, 085207(16) (2008).

[8] M. Zeman and J. Krc, J. Mater. Res. **23**, 889 (2011).

[9] T. Kirchartz, B.E. Pieters, J. Kirkpatrick, U. Rau, and J. Nelson, Phys. Rev. B **83**, 115209 (2011).

[10] T. Kirchartz, Beilstein J. Nanotechnol. **4**, 180 (2013).

[11] M.A. Lampert, Phys. Rev. **103**, 1648 (1956).